Supplementary Information for
Tunable Phase and Fields iSCAT for High-Sensitivity detection of Single Proteins

Ranit Roy[1,2,3], Dushyant Kushavah[1,2,3], Gyanendra Singh[1,2,3], *Ori Cheshnovsky[1,2,3]

1 School of Chemistry, The Raymond and Beverly Sackler Faculty of Exact Sciences, Tel Aviv University, Tel Aviv 69978, Israel

2 Tel Aviv University center for Nanoscience and Nanotechnology

3 Tel Aviv University center for Light Matter Interactions.

Supplementary Note 1: Mathematical Formulation for TPF-iSCAT

Let us define the electric field E associated with the incoming beam defined by the following matrix:

$$E=\begin{bmatrix} E_x \\ E_y \end{bmatrix} \tag{S1}$$

In equation (1), E_x and E_y are the X and Y components of the electric field. Let $E_{r\text{-}p}$ and $E_{s\text{-}p}$ be the polarized reflected and scattered fields in the imaging part; ϕ_r and ϕ_s represents the phase accumulated due to reflection and scattering, mathematically expressed as:

$$E_{r\text{-}p}=\begin{bmatrix} E_r e^{i\phi_r} \\ 0 \end{bmatrix} \qquad E_{s\text{-}p}=\begin{bmatrix} E_s e^{i\phi_s} \\ 0 \end{bmatrix}$$

On passing an Annular Half Wave Plate (A-HWP), which is rotated by 45^0 with respect to the x-axis marked E_r, the fields transform to:

$$E_r=\begin{bmatrix} rE_i e^{i\phi_r} \\ 0 \end{bmatrix} \qquad E_{s\text{-}p}=\begin{bmatrix} 0 \\ sE_i e^{i\phi_s} \end{bmatrix}$$

Here, E_r=rE_i, E_s=sE_i where r is the reflectivity coefficient at the glass medium interface and s is the scattering coefficient and E_i is the incident electric field. The slow axis of the liquid crystal (LC) retarder is made parallel to the scattered beam, E_s, thus on reaching the LC retarder, the field changes to

$$E_r=\begin{bmatrix} rE_i e^{i\phi_r} \\ 0 \end{bmatrix} \quad \text{(S2)} \qquad E_{s\text{-}p}=\begin{bmatrix} 0 \\ E_s e^{i(\phi_s+\phi_{tune})} \end{bmatrix} \quad \text{(S3)}$$

In equation S3, ϕ_{tune} is the phase retarded by the LC Retarder. The reflected and the scattered beam passes through a polarizer next, which has an angle θ with respect to the x-axis, expressed by the following equation:

$$E_r=\begin{bmatrix} rE_i e^{i\phi_r} cos\,(\theta) \\ rE_i e^{i\phi_r} sin\,(\theta) \end{bmatrix} \qquad E_{s\text{-}p}=\begin{bmatrix} sE_s e^{i(\phi_s+\phi_{tune})} sin\,(\theta) \\ sE_s e^{i(\phi_s+\phi_{tune})} cos\,(\theta) \end{bmatrix}$$

Thus, by recording the Y-components due to the polarizer, the interfered terms are given by

$$I_d=|rE_i e^{i\phi_r} sin(\theta)+sE_i e^{i(\phi_{tune}+\phi_s)} cos(\theta)\,|^2$$

$$I_d=\left(rE_i sin(\theta)\right)^2+\left(sE_i cos(\theta)\right)^2+2rsE_i^2 cos(\theta)sin(\theta)cos(\Delta\phi\text{-}\phi_{tune}) \quad \text{(S4)}$$

Equation (4) is the final intensity detected, here $\Delta\phi=\phi_r\text{-}\phi_s$. The polarizer can fine-tune the value of θ, whereas the retardance of the LC Retarder can tune the value of ϕ_{tune}.

Supplementary Note 2: TPF-iSCAT Contrast

The contrast is modelled as introduced in equation 3. iSCAT contrast for a single nanoparticle is given by[1,2]:

$$Contrast=\frac{I_{total}}{I_{ref}}\text{-}1$$

where $I_{total}\ =\ E_s^2+E_r^2+2E_sE_r cos(\Delta\phi)$ and $I_{ref}\ =\ E_r^2$.

For nanoparticles with very low scattering cross-section the terms other than E_r^2, can be safely ignored in the numerator. Using the same contrast model, the TPF-iSCAT contrast can be written as

$$Contrast=\frac{E_s^2 cos^2\theta+E_r^2 sin^2\theta+2E_sE_r cos\,\theta\,sin\,\theta\,cos(\Delta\phi+\phi_{\mathrm{tune}})}{E_r^2 sin^2\theta}\text{-}1=\frac{E_s^2 cos^2\theta+2E_sE_r cos\,\theta\,sin\,\theta\,cos(\Delta\phi+\phi_{\mathrm{tune}})}{E_r^2 sin^2\theta}$$

For particles where there is a large contribution of pure scattering signal, the general contrast is given by:

$$Contrast=\frac{E_s^2 cos^2\theta}{E_r^2 sin^2\theta}+\frac{2E_sE_r cos\,\theta\,sin\,\theta\,cos(\phi+\phi_{\mathrm{tune}})}{E_r^2 sin^2\theta}=\frac{E_s^2}{E_r^2}cot^2\theta+\frac{2E_s}{E_r}cot\,\theta\,cos(\phi+\phi_{\mathrm{tune}}) \quad \text{(S5)}$$

This general form fits well for the data Fig. 2a

For small particles and the system, we consider $E_s cos(\theta) \ll E_r sin(\theta)$ leading to

$$Contrast = \frac{2E_s}{E_r} cot\,\theta\, cos(\phi + \phi_{\text{tune}}) \tag{S6}$$

Supplementary Note 3: Detailed Optical Setup

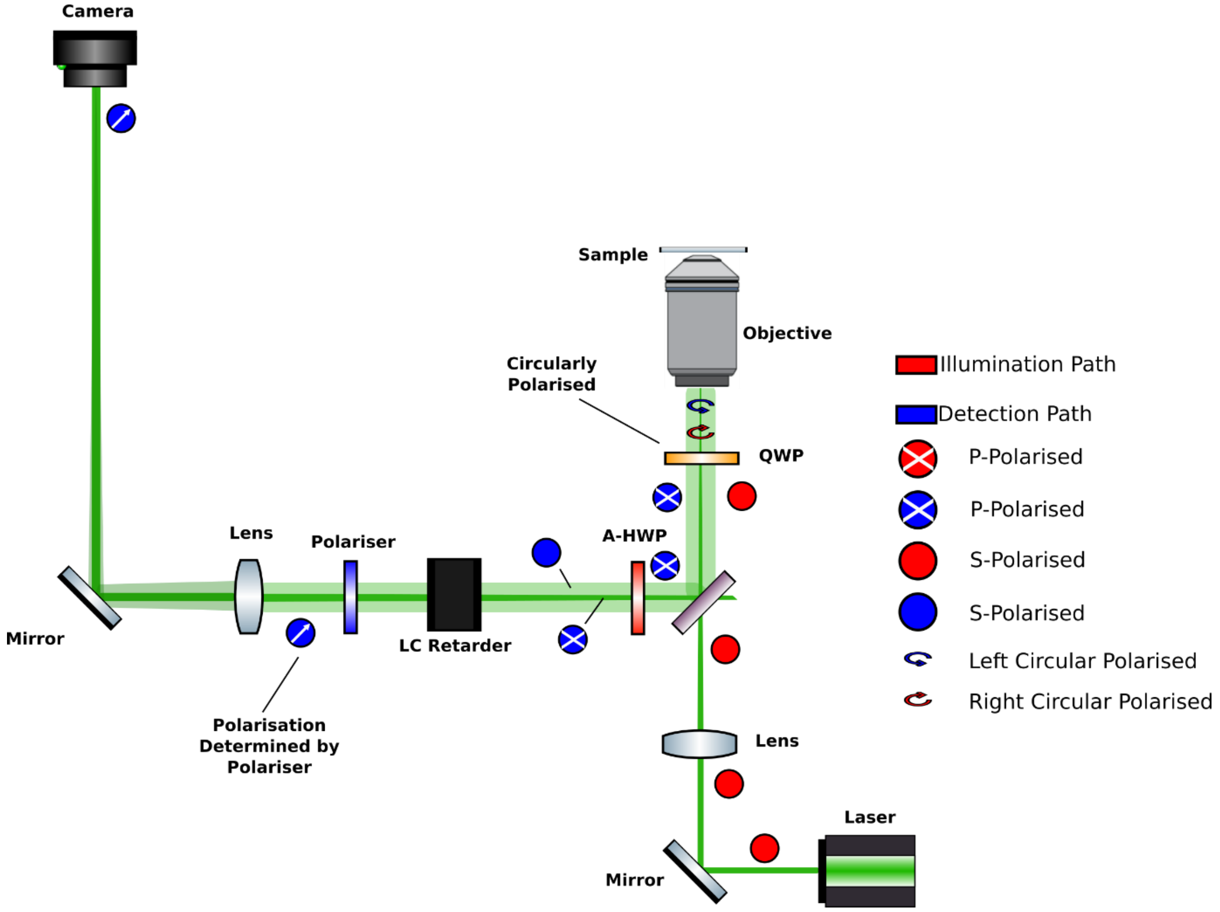

Fig S1: Detailed optical layout of TPF-iSCAT

Supplementary Note 4: Image Generation

Differential ratiometric running average processing was used to extract weak scattering signals of nanostructure from the dominate speckled background generated in iSCAT. In TPF-iSCAT, the acquired frames are divided into two phase channels corresponding to two LC retarder phase states. The frames in the first phase are marked as f_i, while the frames for the second phase are marked as g_i. These frame sets are processed independently and generate separate ratiometric image sequences. The frames are acquired alternatively in time given by

$$f_1(t_0), g_1(t_0 + \Delta t), f_2(t_0 + 2\Delta t), g_2(t_0 + 3\Delta t), \dots$$

Where, Δt is the frame interval. The acquisition is synchronized by a fixed external trigger. The complete acquisition and processing sequence to the final image generation has shown schematically in Fig S2.

For the first phase channel name, a reference image by averaging N frames during the interval $[0, t]$.

$$A_i^{(P1)} = \frac{1}{N} \sum_{k=i}^{i+N-1} f_k$$

For the second image windows by averaging the next N frames during the interval $[t, 2t]$.

$$A_{i+1}^{(P1)} = \frac{1}{N} \sum_{k=i+N}^{i+2N-1} f_k$$

The ratiometric generate for this phase state would be given by

$$\tilde{C}_i^{(P1)} = 1 - \frac{A_{i+1}^f}{A_i^f}$$

For the second phase channel name, a reference image by averaging N frames.

$$A_i^{(P2)} = \frac{1}{N} \sum_{k=i}^{i+N-1} g_k$$

For the second image windows by averaging the next N frames.

$$A_{i+1}^{(P2)} = \frac{1}{N} \sum_{k=i+N}^{i+2N-1} g_k$$

The ratiometric generate for this phase state would be given by

$$\tilde{C}_i^{(P2)} = 1 - \frac{A_{i+1}^{(P2)}}{A_i^{(P2)}}$$

As, the acquisition proceeds, the averaging window keeps translating over the next subsequent frames in the independent frame sequences given by $P1$ and $P2$. They produce temporal ratiometric image streams given by $\tilde{C}_i^{(P1)}$ and $\tilde{C}_i^{(P2)}$.

The images generated using DRA are separated into two phase channels which correspond to two LC retarder phase states. The DRA frames acquired for the first phase are given by $C_i^{(P1)}$, while the frames acquired by the second phase are given by $C_i^{(P2)}$. The contrast images form a quadrature pair. The maximum contrast extracted from this quadrature pair is the vector magnitude given by

$$C_{max} = \sqrt{(C_i^{(P1)})^2 + (C_i^{(P2)})^2}$$

The phase obtained from the relative values of the contrast components would be given by

$$\Delta\phi = arctan\left(C_i^{(P2)}, C_i^{(P1)}\right)$$

The conversion of the contrast maps into the extracted amplitude and the phase extraction

Supplementary Note 5: Data Collection Procedure

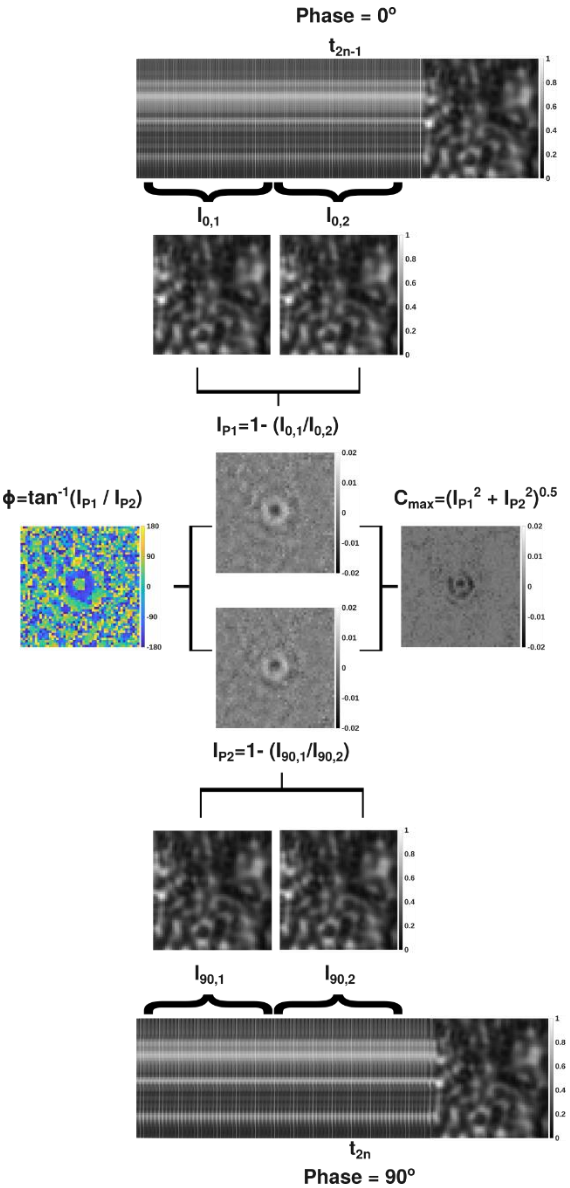

Fig S2: Schematic of the TPF-iSCAT data processing pipeline. Frames acquired at a phase offset of 0^0 correspond to odd-indexed acquisition times t_{2n-1}, whereas for 90^0 correspond to even-indexed acquisition times t_{2n}. For each applied phase, which we acquire alternatively between 0^0 and 90^0 using a delay generator, as shown in Supplementary Note 5, we partitioned raw image sequences into first and second temporal windows and averaged to generate $I_{0,1}$, $I_{0,2}$, $I_{90,1}$ and $I_{90,2}$. The normalised differential images $I_{P1} = 1 - (I_{0,1}/I_{0,2})$ and $I_{P2} = 1 - (I_{90,1}/I_{90,2})$ They were used to extract the phase, $\Delta\phi = \tan^{-1}(I_{P1}/I_{P2})$, and the maximum contrast amplitude, $C_{max} = \tan^{-1}(I_{P1}^2 + I_{P2}^2)^{0.5}$.

Supplementary Note 6: Acquisition Time and LC Retarder Response

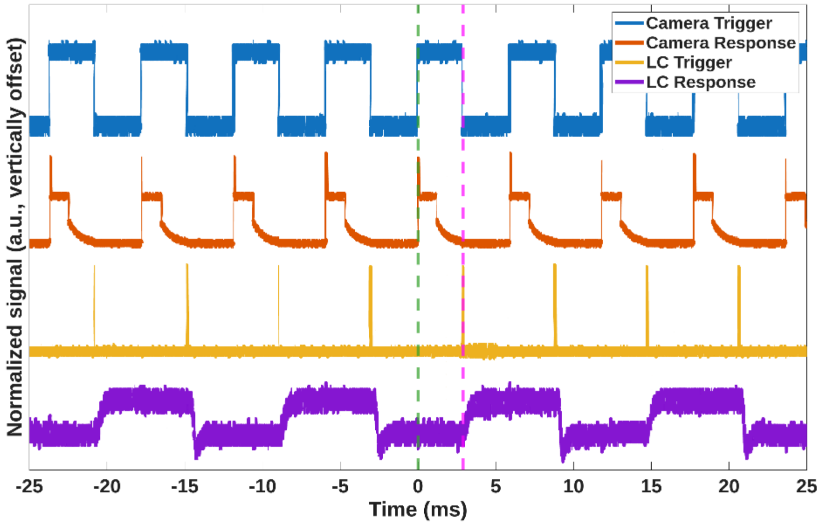

Fig S3: Normalized, vertically offset oscilloscope traces showing the timing relationship between the camera and liquid-crystal (LC) control signals. The camera trigger (blue) and camera response (orange) are plotted together with the LC trigger (yellow) and LC response (purple). Dashed vertical lines mark the reference time (0 ms, green) and the LC response delay (2.90 ms, magenta). The signal was generated at a speed of 169 Hz. The initial spike and the extended tail following the end of the square wave response in the camera output are inherent to the camera itself.

The LC retarder effectively sets the acquisition speed of the system through its voltage switching and phase transition dynamics. For imaging small proteins, a highly stable background is required, since the weak scattering contrast is otherwise obscured by phase transition induced background fluctuations. To ensure that the background used for differential running average is not corrupted by these transient variations, the acquisition is intentionally slowed to allow the LC retarder to settle between states, yielding stable backgrounds suitable for subtraction.

Supplementary Note 7: System Stability

The sensitivity of TPF-iSCAT is set by the system noise floor. In standard iSCAT without a reflectivity-reduction mask, the high reflected photon flux allows photon shot-noise limited performance to be reached at relatively low frame averaging. In contrast, introducing a reflectivity-reduction mechanism lowers the available photon flux; consequently, at higher running averages, the measured noise becomes increasingly dominated by technical noise sources rather than shot noise. To mitigate this limitation, TPF-iSCAT is implemented with acoustic and thermal isolation and supplemented with laser stabilisation measures. As a result, the standard deviation as a function of running average is reduced to the level shown below:

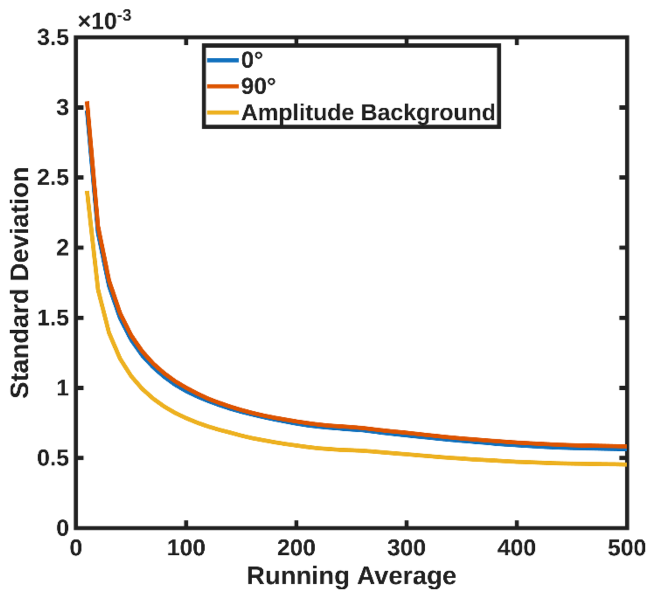

Fig S4: Standard Deviation (SDV) of the background as a function of running-average window length for two phase settings (0° and 90°), with the corresponding amplitude-background estimate shown for comparison. A stable background movie was recorded; running averages were computed using multiple window sizes. For each window size, the SDV of the averaged background was calculated and the median SDV value is plotted versus window length. Increasing the averaging window reduces the background noise and approaches a steady value for large window sizes.

Supplementary Note 8: Table of Data

Tables

Table S1: Gold Nanoparticle Histogram Data

Gold Particle Size	Phase = 0^0	Phase = 90^0	C_{max}	Extracted Phase
2nm	0.006 ± 0.0014	0.0059 ± 0.0016	0.0084 ± 0.0020	45 ± 5.7º
5nm	0.0061 ± 0.0016	0.0068 ± 0.0018	0.0092 ± 0.0026	47 ± 5.13°
10nm	0.0147 ± 0.0080	0.013 ± 0.0085	0.019 ± 0.0103	44 ± 4.7°
15nm	0.029 ± 0.011	0.026 ± 0.012	0.039 ± 0.015	43.7 ± 3.2°

Table S2: Protein Histogram Data

Proteins	Phase = 0^0	Phase = 90^0	C_{max}	Extracted Phase
Bovine Insulin	0.00356 ± 0.00066	0.0038 ± 0.0009	0.00484 ± 0.0010	-132 ± 8.05°
Horse Heart Myoglobin	0.0037 ± 0.0016	0.0036 ± 0.0013	0.00502 ± 0.0017	-135 ± 7.12°
Green Fluorescent Protein	0.0039 ± 0.0008	0.0038 ± 0.0011	0.00512 ± 0.0014	-134 ± 8.32°
Bovine Serum Albumin	0.00463 ± 0.0013	0.00456 ± 0.0012	0.00606 ± 0.00173	-133 ± 6.32°
Malate Dehydrogenase	0.00457 ± 0.0015	0.0047 ± 0.0013	0.0061± 0.0019	-133 ± 6.89°

References

1. Taylor, R. W. *et al.* Label-free, ultrasensitive, ultrahigh-speed scattering-based interferometric imaging. *Opt. Commun.* **13**, 480–487 (2018).
2. Cole, D., Young, G., Weigel, A., Sebesta, A. & Kukura, P. Label-Free Single-Molecule Imaging with Numerical-Aperture-Shaped Interferometric Scattering Microscopy. *ACS Photonics* **4**, 211–216 (2017).